Tau Induces Ring and Microtubule Formation from R*â*-Tubulin Dimers under Nonassembly Conditions[2]

François Devred,[3] Pascale Barbier,[3] Soazig Douillard,[3] Octavio Monasterio,[§] José Manuel Andreu,[|] and Vincent Peyrot*,[3]

FRE 2737, ISPDCT, Faculté de Pharmacie, 27 Bd Jean Moulin, 13385 Marseille Cedex 5, France, Departamento de Biologia, Facultad de Ciencias, Universidad de Chile, Casilla 653, Santiago, Chile, and Centro de Investigaciones Biologicas, Consejo Superior de Investigaciones Cientificas, Ramiro de Maeztu 9, 28040 Madrid, Spain

Received April 7, 2004; Revised Manuscript Received June 11, 2004

ABSTRACT: Tau is a neuronal microtubule-associated protein that plays a central role in many cellular processes, both physiological and pathological, such as axons stabilization and Alzheimer's disease. Despite extensive studies, very little is known about the detailed molecular basis of tau binding to microtubules. We used the four-repeat recombinant htau40 and tubulin dimers to show for the first time that tau is able to induce both microtubule and ring formation from 6S R*â* tubulin in phosphate buffer without added magnesium (nonassembly conditions). The amount of microtubules or rings formed was protein concentration-, temperature-, and nucleotide-dependent. By means of biophysical approaches, we showed that tau binds to tubulin without global-folding change, detectable by circular dichroism. We also demonstrated that the tau−tubulin interaction follows a ligand-mediated elongation process, with two tau-binding site per tubulin dimer. Moreover, using a tubulin recombinant R-tubulin C-terminal fragment (404−451) and a *â*-tubulin C-terminal fragment (394−445), we demonstrated the involvement of both of these tubulin regions in tau binding. From this model system, we gain new insight into the mechanisms by which tau binds to tubulin and induces microtubule formation.

The microtubule cytoskeleton is a very dynamic network that plays a crucial role in many cellular processes such as cellular architecture, cell division, and intracellular traffic. Microtubule dynamic instability and functions are regulated by microtubule-associated proteins (MAPs).[1] Tau is a MAP that stabilizes axonal microtubules and maintains neuronal processes (*1*). Tau is also known to play a major role in Alzheimer's disease (see ref *2* for review). Detached from microtubules by phosphorylation, tau may aggregate to form pathological paired helical filaments (PHFs) upon further hyperphosphorylation (see ref *3* for review). Recently, it has also been suggested that tau could play a role in Alzheimer's disease long before it detaches from microtubules and aggregates (*4*, *5*). Thus, tau binding to microtubules plays a pivotal role in both pathological and physiological processes.

Tau−microtubule interactions have been investigated intensively, leading to the identification of tau and tubulin regions implicated in this interaction. Each tau isoform contains three to four microtubule-binding repeats, located in its C-terminal part. The first inter-repeat (*6*, *7*), as well as the flanking domains (*8*, *9*), enhances the binding affinity of these repeats. For tubulin, except for one study that showed that the N-terminal peptide R(1−75) was able to bind tau (*10*), most of the studies showed that tau, just like the others MAPs, binds in the C-terminal region of tubulin (*11*−*13*). Recently, it was shown that tau binds to two distinct sites on the C-terminal part of tubulin, one of which is located within the 12 C-terminal amino acids of both R and *â* tubulin (*14*). Using taxol-stabilized microtubules, Al-Bassam et al. (*15*) concluded that tau binds longitudinally along the outer ridges of protofilaments, probably on tubulin H11 and H12 helices. More recently, in a study performed in the presence of TMAO, known to enhance tau activity on tubulin assembly, Kar et al. (*16*) proposed that tau would also bind to the inside of the microtubule wall. It has also been suggested that tau undergoes a complex intramolecular rearrangement upon binding to microtubules (*9*, *17*).

On the basis of these results, several models have been proposed to explain how tau proteins interact with microtubules. According to the most prevailing model, tau would overlap along several tubulin dimers or across the protofilaments (*8*, *18*−*20*). This model presumes that each repeat and

[2] Part of this work was supported by the ARC Grant 7264, the Ligue Contre le Cancer (2000−2001), Gefluc Marseille-Provence, MCyT Bio 2002-03665 Grant, and PAI Picasso Grant 07074PH.

* To whom correspondence should be addressed. Telephone and fax: (33) 491835505. E-mail: vincent.peyrot@pharmacie.univ-mrs.fr.

[3] Faculté de Pharmacie.

[§] Universidad de Chile.

[|] Consejo Superior de Investigaciones Cientificas.

[1] Abbreviations: AUC, analytical ultracentrifugation; CD, circular dichroism; Cr, critical concentration; EM, electron microscopy; MAP, microtubule-associated protein; MES, 2-(*N*-morpholino)ethanesulfonic acid; PEMGT buffer, 3.4 M Glycerol, 20 mM sodium phosphate, 1 mM EGTA, 10 mM Mg^{2+}, 0.1 mM GTP, and 1 mM TCEP at pH 6.5; PGT buffer, 20 mM sodium phosphate, 10^{-4} or 10^{-5} M GTP, and 1 mM TCEP at pH 6.5; PIPES, piperazine-*N*,*N*-bis(ethanesulfonic acid); PT buffer, 20 mM sodium phosphate and 1 mM TCEP at pH 6.5; SDS−PAGE, sodium dodecyl sulfate polyacrylamide gel electrophoresis; SEC, size-exclusion chromatography; TCEP, tris(2-carboxyethyl)phosphine; TFA, trifluoroacetic acid; TFE, trifluoroethanol; TMAO, trimethylamine-*N*-oxyde.

inter-repeat region interacts with a separate but adjacent tubulin monomer within the microtubule wall. However, some studies suggest that tau would not necessarily need to overlap several tubulin dimers to stabilize microtubules (*14*, *17*, *21*, *22*).

Many studies addressed the issue of stoichiometry, binding affinity, and geometry of tau binding to microtubules; however, results obtained in different conditions lead to different conclusions, and so far no unifying scheme was proposed. Furthermore, the question whether tau acts as a stabilizing agent by binding to the microtubules wall or as a true assembly inducer from tubulin dimers remains unresolved. To investigate the mechanisms by which tau binds to microtubules and/or to R*â*-tubulin dimers, we used an environment depleted of assembly promoters such as taxol, TMAO, or Mg^{2+}. For the first time, we showed that four-repeat tau is a true microtubule assembly inducer. In nonassembly conditions, tau was able to induce either microtubule or tubulin ring formation depending on the temperature and GTP concentration. We showed that microtubule formation follows a ligand-mediated elongation process and gave an estimation of the tau−tubulin binding constant, the elongation constant, and the stoichiometry. Using two tubulin C-terminal peptides R(404−451) and *â*-(394−445), from the main tubulin vertebrate isotypes (*23*), we also demonstrated the interaction of tubulin H12 and newly described H11 (*24*) C-end regions in tau binding. Finally, we showed that tau binds to tubulin without global-folding change, detectable by circular dichroism (CD). These results provide new insight into the tau mechanism of action, which is a central issue for both neurodegenerative processes and neuron stabilization.

EXPERIMENTAL PROCEDURES

Tubulin Purification and Expression of R *and â C-Terminal Domains.* Tubulin was purified from lamb brains by ammonium sulfate fractionation and ion-exchange chromatography and stored in liquid nitrogen as described (*23*, *25*, *26*). Tubulin concentration was determined spectrophotometrically at 275 nm with an extinction coefficient of 109 000 M^{-1} cm^{-1} in 6 M guanidine hydrochloride. R tubulin fragment RL52R3 (termed CR throughout) consists of the 48 C-terminal residues of R tubulin (404−451) (isotype hkR1), whereas the *â* tubulin construct RL33*â*6 (termed C*â* throughout) consists of the 52 C-terminal residues of *â* tubulin (394−445) (isotype c*â*2), preceded by the amino acid sequence ARIRAP from the plasmid construction. Expression, purification, and peptide concentration determination using an extinction coefficient of 9530 M^{-1} cm^{-1} at 280 nm was performed as previously described (*23*).

Tau Expression and Purification. The four-repeat 441 amino acids isoform of tau, htau40 (termed tau throughout), was expressed from a pET vector (kindly provided by M. Goedert) introduced into *Escherichia coli* BL21(DE3). Tau expression was induced by the addition of 0.5 mM isopropyl 1-thio-*â*-D-galactopyranoside (IPTG) to cells when A_{600nm} reached 0.6. A total of 3 h after induction at 37 °C, cells were pelleted and resuspended in purification buffer [50 mM MES, 1 mM DTT, 1 mM PMSF, and 5 mM EDTA (pH 6.5)]. After two runs in the French press (6 tones), the lysate was cleared by a centrifugation 25 000 rpm for 30 min at 4 °C and then precipitated with 45% ammonium sulfate for 10 min at 4 °C. It was then recentrifuged, and the pellet was resuspended in purification buffer and dialyzed against a buffer containing 50 mM MES, 1 mM TCEP, 1 mM EGTA, and 5 mM EDTA (pH 6.5) overnight. After the solution was cleared by centrifugation, the supernatant was loaded onto a HiTrap SP Sepharose HP cation exchange column (Amersham Pharmacia) pre-equilibrated with a buffer containing 50 mM MES at pH 6.5 and then eluted at 0.5 mL min^{-1} with a buffer containing 50 mM MES and 0.5 M NaCl at pH 6.5. Further purification was achieved using a SourceTM 15RPC PE 7.5/150 (Amersham Pharmacia) reverse-phase column equilibrated with H_2O TFA (0.065%), on which fractions containing tau were loaded and eluted with Acetonitrile TFA (0.05%). Fractions containing tau were then pooled and dry-lyophilized. Tau was weighted and resuspended before use. The tau concentration was measured at 280 nm using an extinction coefficient of 7700 M^{-1} cm^{-1} as calculated with antheprot (*27*) and then checked by amino acid composition.

Tau and Tubulin/Tubulin Peptide Interaction. In nonassembly conditions, tubulin was prepared by equilibrating the tubulin on a cold Sephadex G25 medium (1 × 20 cm) equilibrated with an appropriate buffer. Experiments were performed in a PT buffer (20 mM sodium phosphate and 1 mM TCEP at pH 6.5) with 10^{-4} or 10^{-5} M GTP, when needed (in the presence of tubulin). In assembly conditions, tubulin was prepared as described previously (*28*) in a PEMGT buffer (3.4 M glycerol, 20 mM sodium phosphate, 1 mM EGTA, 10 mM Mg^{2+}, 0.1 mM GTP, and 1 mM TCEP at pH 6.5).

Cosedimentation Assay and Gel Analysis. Samples (125 *í*L) were centrifuged using a TL-100 Beckman ultracentrifuge with a TLA 100.2 rotor during 15 min at 50 000 rpm at 37 °C to pellet microtubules. Polyacrylamide gel electrophoresis in denaturing conditions (SDS−PAGE) was performed using 15% acrylamide in the separating gel and Amersham Pharmacia low-weight calibration kit (97, 66, 45, 30, 20.1, and 14.4 kDa) for standards. Gels were stained with Coomassie Brilliant Blue. The protein quantification and molar ratio of tubulin dimer to tau were performed using Traitima.exe, image-analysis software provided by Dr. Sarrazin (marcel.sarrrazin@pharmacie.univ-mrs.fr). The assay was performed 3 times. In the absence of tubulin, tau never sedimented to more than a few percents and neither did tubulin in the absence of tau.

Spectroscopic Measurements. Light absorption spectra were obtained with a Perkin−Elmer Lambda 800 UV−vis spectrometer. Fluorescence measurements were obtained with a Kontron SFM 25 luminescence spectrometer 50, with slit widths of 5/5 nm, using 0.2 (excitation direction) × 1 cm (emission direction) cells (Hellma), thermostated at 25 °C. The excitation was done at 275 nm or at 295 nm to specifically excite tryptophans. Note that, at the concentrations used, spectra gave no appreciable inner-filter effect ($A < 0.05$).

CD Spectra. CD spectra of tau, tubulin, and peptides were acquired with a Jasco 720 spectropolarimeter using cuvettes from 0.1 to 1 mm optical path. Spectra of the tau−tubulin mixture were recorded with a 0.5 nm step at 20 nm min^{-1} speed, as an average of 5 scans, and corrected for the baseline. Spectra of the tau−tubulin peptide mixture were

recorded with a 1.0 nm step at a 20 nm min^{-1} speed, as an average of 4 scans, and corrected for the baseline. All of these measurements are reported as ellipticity $\tilde{o}$ (millidegrees). The secondary structure analysis of the CD data was performed as previously described using Dicroprot (*27*).

Exclusion Chromatography. Size-exclusion chromatography experiments were performed at room temperature using an AKTA–HPLC system (Amersham Pharmacia Biotech). Samples were loaded on a Superdex 200 HR10/30 column (Amersham Pharmacia Biotech) pre-equilibrated in the same buffer as the samples, except for the measurement of the Stokes radius of tau, where the PT buffer was supplemented with 500 mM NaCl. Fractions of 0.2–1 mL were collected at a flow rate of 0.5 mL min^{-1}, and absorbances were measured at 280 and 215 nm. For calibration, we used proteins with known Stokes radii and molecular masses. The standards were ferritin (MW) 232 kDa, R_s) 61 Å), catalase (MW) 232 kDa, R_s) 52.2 Å), aldolase (MW) 158 kDa, R_s) 48.1 Å), albumin (MW) 67 kDa, R_s) 35.5 Å), chymotrypsinogen A (MW) 25 kDa, R_s) 20.9 Å), and RNase A (MW) 13.7 kDa, R_s) 16.4 Å).

Analytical Ultracentrifugation: Sedimentation Equilibrium. Experiments were performed with a Beckman Optima XL-A analytical ultracentrifuge equipped with absorbance optics, using an An55Ti rotor. A short column sedimentation equilibrium experiment was performed on 60 *i*L of tau, with a loading concentration ranging from 1.5 to 4.5 mg/mL in the six-channel centerpieces of charcoal-filled Epon. Measurement was done at three successive speeds (8000, 10 000, and 14 000 rpm) by taking scans at the appropriate wavelength (275 and 250 nm) when sedimentation equilibrium was reached. The temperature was 20 °C. High-speed sedimentation was conducted afterward for baseline correction. Average molecular masses were determined by fitting a sedimentation equilibrium model for a single sedimenting solute to individual data sets with XLAEQ and EQASSOC supplied by Beckman (*29*). Data analysis was also performed by global analysis of several data sets obtained at different loading concentrations using MULTEQ3B (*29*) and NONLIN (*30*). The partial specific volume of tau was 0.721 mL/g, calculated from the amino acid composition by SEDNTERP (*31*).

Sedimentation Velocity: Tau Characterization. Experiments were carried out at 55 000 rpm and 20 °C in the same XL-A instrument, using 12 mm aluminum double-sector centerpieces. Data were acquired in continuous mode at 275 nm. Apparent sedimentation coefficients were determined using SEDFIT (*32*) and were corrected to standard conditions using SEDNTERP (*31*).

The frictional coefficient ratio (f/f_0) was calculated using f/f_0) s_{max}/s, where f_0 and s_{max} are the frictional and sedimentation coefficients of a smooth unhydrated sphere corresponding to the given protein mass, s is the experimental sedimentation coefficient obtained by UCA, and f is the frictional coefficient of the protein (*33*).

Tau–Tubulin Interaction. Experiments were carried out at 30 000 and 40 000 rpm at 20 °C using 12 mm charcoal-filled Epon centerpieces. Data were acquired in continuous mode at 275 nm. The distributions $g(s^*)$ were generated by least-squares boundary modeling of sedimentation velocity data by DCDT$^+$ (*34*, *35*). These distributions were then fitted with Gaussian curves, and the areas and maximum, which represent the sediment coefficient of the sample, were calculated. We used this analysis to qualitatively characterize the tau–tubulin interaction; the boundaries do not represent individual species but interacting zones.

In AUC, experiments were performed in 10^{-5} M GTP. The nucleotide composition of the tubulin was determined to be mainly GTP tubulin (87%), which is not significantly different from the GTP tubulin equilibrated with 10^{-4} M GTP buffer (90%).

The solvent density and the viscosity were calculated with SEDNTERP; they were 1.000 58 g/cm^3 and 0.010 469 poise, respectively (at 20 °C).

Models of Ligand-Induced Macromolecular Self-Association. Ligand-induced tubulin assembly may proceed by two different pathways (*36*): either a ligand-facilitated elongation pathway, in which the elongation precedes the binding of the ligand (eq 1) or a ligand-mediated elongation pathway,

$$\mathrm{MT} + \mathrm{Tub} \overset{K_2}{\rightleftharpoons} \mathrm{MT-Tub} + \mathrm{X} \overset{K_1}{\rightleftharpoons} \mathrm{MT-Tub-X} \quad (1)$$

in which the binding of tau (noted X), to either tubulin or microtubule, precedes the elongation (eq 2 and 2). Equation 1

$$\mathrm{X} + \mathrm{Tub} \overset{K_1}{\rightleftharpoons} \mathrm{Tub-X} + \mathrm{MT} \overset{K_2}{\rightleftharpoons} \mathrm{MT-Tub-X} \quad (2)$$

$$\mathrm{MT} + \mathrm{X} \overset{K_1}{\rightleftharpoons} \mathrm{MT-X} + \mathrm{Tub} \overset{K_2}{\rightleftharpoons} \mathrm{MT-Tub-X} \quad (2')$$

is characterized by an apparent elongation constant K_{app}) $K_2(1 + K_1X)$. Equations 2 and 2 are not thermodynamically discernible and are characterized by an apparent elongation constant K_{app}) $K_1K_2X/(1 + K_1X)$ (for more details, see the appendix of ref *37*). In the case of a two-ligand-mediated elongation process, the apparent elongation constant becomes K_{app}) $K_1 K_2 X^2/(1 + K_1 X^2)$. All of the fittings were done using a graphics-fitting program (Sigmaplot 4.0, Jandel Scientific).

Miscellaneous. Residual Mg^{2+} concentration was determined by atomic absorption spectroscopy (*38*, *39*).

Nucleotide content measurement was performed as previously described (*40*) with minor modifications. Samples of 900 *i*L, precipitated with perchloric acid (3%) in the presence of an additional 1 *i*M GMP as an internal standard, were centrifuged in a Heraeus Sepatech Biofuge A at maximum speed (13 000 rpm) for 10 min at 4 °C. Supernatants were then neutralized to pH 8.0 using 3 M NaOH and loaded on a Nucleosil 4000.7 PE column pre-equilibrated with 10 mM Tris/HCl at pH 8.2. Nucleotides were then eluted with 20 mM Tris/HCl at pH 8.0 and 1.5 M NaCl. The GTP and GDP ratio was then measured by peak integration.

Electron Microscopy. Samples were adsorbed onto 200 mesh, Formvar carbon-coated copper grids, stained with 2% (w/v) uranyl acetate, and blotted to dryness. Grids were observed using a JEOL JEM-1220 transmission electron microscope operated at 80 kV. Magnifications used ranges from 20001 to 500001. To ensure that microtubules do not disassemble during adsorption, this step was performed in a thermostated room at 37 °C, unless stated otherwise.

RESULTS

Characterization of Purified Recombinant hTau40. Recombinant tau was purified without heat treatment because

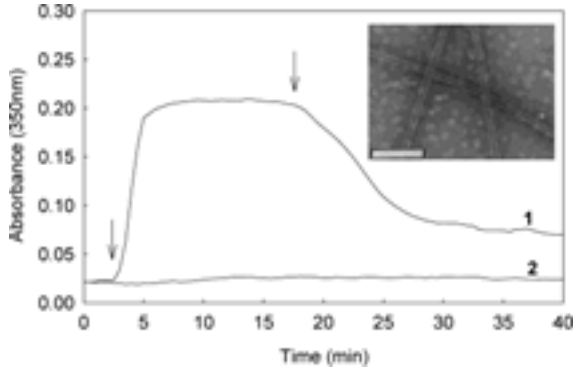

FIGURE 1: Effect of tau on tubulin assembly. Tubulin (5 μM) was incubated at 37 °C in PEMGT buffer. At the time indicated by the first arrow, tau (5 μM) was added to the sample (line 1), whereas buffer was added to the control (line 2). At the time indicated by the second arrow, samples were cooled to 9 °C. (Inset) Electron micrographs of tau-induced microtubules at the plateau. The bar represents 200 nm.

it has been shown that boiling affects the tau structure (*41*). Because tau has a high tendency to oligomerize in non-reducing conditions (*42*), we conducted the whole study in the presence of a stable reducing agent (1 mM TCEP). As evidenced by SDS−PAGE analysis (data not shown), the protein was 98% homogeneous and behaved as an apparent 66 500 Da species, in agreement with what has been reported (*1*). Using mass spectrometry, we found a single sharp peak at 45 718 ± 50 Da (theoretical 45 850 Da), indicating that the first methionine residue had been cleaved because of the bacterial expression, which was confirmed by N-terminal sequencing.

Tau is known to promote tubulin assembly into microtubules (*43*). To check the functionality of our tau preparation, we tested its activity on tubulin assembly in vitro, in PEMGT buffer (*28*). In these conditions, the critical concentration (Cr) under which no tubulin assembly occurs is 7.0 μM (*17*). Figure 1 shows that, in the presence of tau, tubulin polymerizes below this threshold. The turbidity generated by the assembly of tubulin increases in the presence of tau at 37 °C and decreases when the sample was cooled to 9 °C, indicating the reversibility of the process. At the plateau, electron microscopy revealed the presence of morphologically normal microtubules (inset of Figure 1). Tau induced and stabilized microtubule formation; therefore, it is functional and can be further characterized in solution.

By far-UV CD, we found that tau had little secondary structure compatible with 6% helix, 15% sheet, and 12% turn. This is consistent with the earlier studies revealing a mostly random-coil conformation of tau (*1*, *44*). Nevertheless, this could also be due to some unusual secondary structure elements such as poly(L-proline) II helical conformation (*45*).

To characterize the quaternary structure of tau in solution, we performed Superdex S200 size-exclusion chromatography

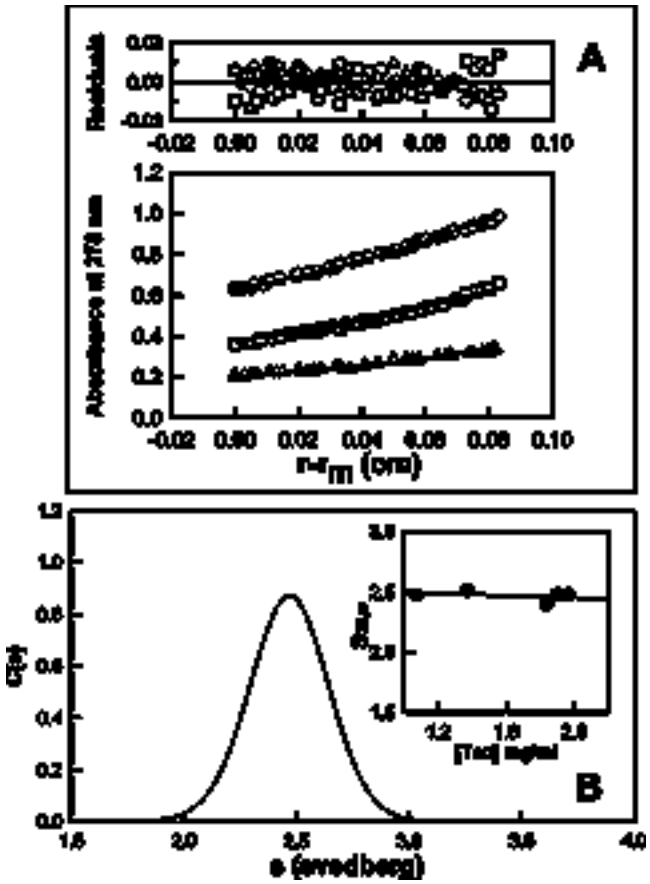

FIGURE 2: Tau characterization by AUC. (A) Sedimentation equilibrium analysis of tau at 20 °C. The symbols show the experimental radial distribution of tau at sedimentation equilibrium at 1.5 mg mL^{-1} (4), 3 mg mL^{-1} (O), and 4.5 mg mL^{-1} (O). The solid lines represent the best fit curves of global analysis of multiple sedimentation equilibrium data with the single, ideal species model. Of nine fitted data sets (the three protein concentrations indicated above at three speeds: 10 000, 12 000, and 16 000 rpm) only three (the ones at 16 000 rpm) are shown. The r_m is the radial distance at the meniscus, with the residuals representing the variation between the experimental data and those generated by the fit with single species. (B) Continuous sedimentation coefficient distribution $C(s)$ of tau at 1.9 mg mL^{-1} at 20 °C. Inset shows the dependence of the apparent sedimentation coefficient at 20 °C in water.

(SEC) and analytical ultracentrifugation (AUC) experiments. Results are summarized in Table 1. SEC analysis showed that the protein was eluted as a single sharp peak with a Stokes radius of 44 Å. This radius is too large for a globular monomer with a molecular mass of 45 719 Da. It could either correspond to a tetramer or to a extended protein, because estimation of molecular weight from SEC is only suitable for globular protein (*46*). Thus, to determine the association state of tau, sedimentation equilibrium experiments were performed using three initial loading concentrations of tau and three rotor speeds (Figure 2A). Fitting the three

Table 1: Hydrodynamic Parameters of Human Tau 40

MM (Da)	44 000 ± 5000	measured by AUC (sedimentation equilibrium)
$S°_{20,w}$[a] (S)	2.5 ± 0.1	measured by AUC (sedimentation velocity)
f/f_0[b]	1.81	calculated by AUC (sedimentation velocity)
R_s[c] (Å)	42	calculated by AUC
	44	determined by size exclusion chromatography
$D_{20,w}$[d] (cm^2/s)	2.39 × 10^{-7}	

[a] $S°_{20,w}$ is the corrected sedimentation coefficient at 20 °C in water for infinite dilution. [b] f and f_0 are the frictional coefficients. [c] R_s is the Stokes radius. [d] $D_{20,w}$ is the corrected diffusion coefficient.

concentration data sets simultaneously at one speed (16 000 rpm) showed that the best residual distribution, and the minimum square root of variance was obtained for a single ideal species model (Figure 2A). We found a value of 44 000 ◐ 5000 Da, in agreement with the theoretical molecular mass of the monomer of tau. Sedimentation velocity experiments confirmed the monodisperse nature of tau in solution by the presence of a single sharp boundary, at any concentration used. The sedimentation coefficient distribution $C(s)$ showed a single symmetrical peak centered at 2.57 S (Figure 2B), indicating the presence of a single species.

The tau sedimentation coefficient decreased with concentration, as expected for a nonassociative single particle (inset of Figure 2B). A $s^0_{20,w}$ of 2.5 ◐ 0.1 S was obtained at infinite dilution in water. Using this sediment coefficient value, we calculated (see the Experimental Procedures) the frictional coefficient ratio (f/f_0) of tau to be 1.81 and the Stokes radius, 42 Å (Table 1). This frictional coefficient ratio is higher than 1.6, which corresponds to a moderately elongated protein (*33*). Indeed, the sedimentation coefficient of tau 2.5 S is larger than the value expected for a random-coil polypeptide chain of the same length, $s^0_{20,w}$ 1.4 S (*47*), implying some residual restriction to a complete unfolding of tau in a buffer.

After concluding that tau was pure, functional, and monomeric in reducing conditions, we were able to study tau interaction with R−â tubulin dimers.

Analysis of Tau−Tubulin Interaction at 20 °C. Most of the previous experiments to study tau binding to microtubules or tubulin were performed either with stabilized microtubules or with peptides corresponding to small constructs of tau and/or tubulin. To observe the binding of tau to unpolymerized tubulin and to measure potential changes in either tau or tubulin structures, we studied the binding of the entire tau protein to tubulin dimers by AUC under nonassembly conditions. The sedimentation velocity of tubulin was examined at 20 °C in the presence of tau. In our conditions, control tubulin sedimented as a single species as indicated by the single Gaussian distribution of the $g(s^*)$ plot. This distribution was centered on 5.43 ◐ 0.03 S for 15 ¿M tubulin (inset of Figure 3A).

Figure 3A shows a trimodal pattern resulting from the interaction of 15 ¿M tubulin and 7.5 ¿M tau. The $g(s^*)$ distribution, which is very sensitive to the presence of multiple species, was fitted with 3 Gaussian curves centered on 6 S, 30−35 S, and 40−50 S, respectively. To test the nature of the equilibrium, similar experiments were performed at a different speed. They led to the same sedimentation pattern, indicating that this self-associating system was in rapid equilibrium (*48*). Note, however, that the peaks observed by AUC are not individual species but sediment boundaries of this reversible associating system. Apparent sedimentation coefficients (inset of Figure 3B) and amount of the different sediment boundaries (Figure 3B) were calculated by integrating the Gaussian curves obtained for the different peaks (see the Experimental Procedures) for different tau/tubulin molar ratios and different tubulin concentrations. The proportion of the slow peak centered on 6 S decreased in favor of a rapid sedimenting peak centered on 30 S, and then, when the tau/tubulin ratio was raised even more, a third peak centered on 45 S appeared. As we increased the tau/tubulin ratio, the area of the second sedimenting boundary (30 S) increased until it reached 20%

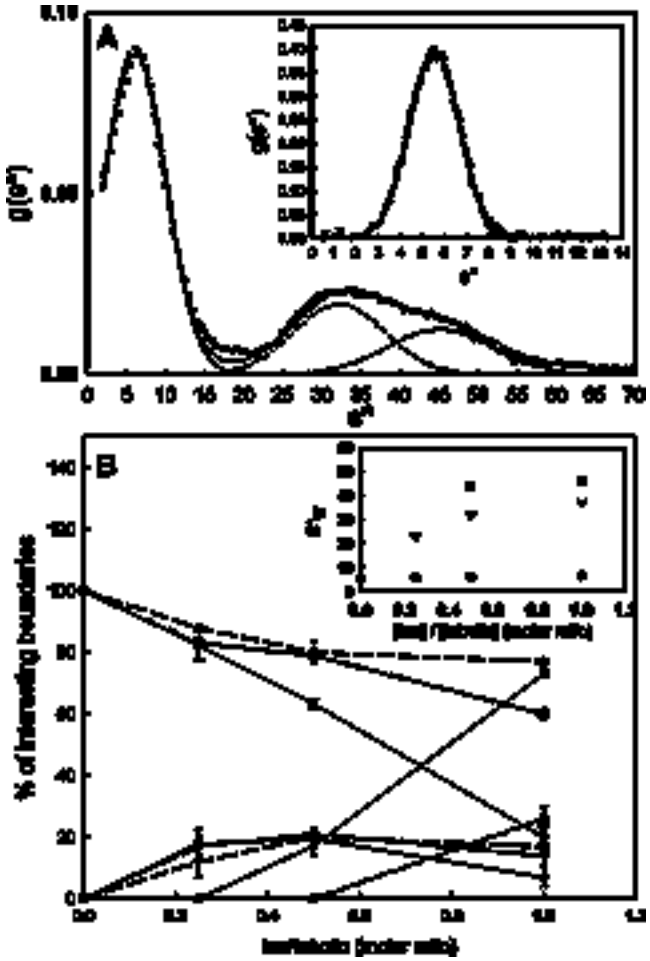

FIGURE 3: Sedimentation velocity of tau−tubulin interaction at 20 °C. (A) Apparent sedimentation coefficient $g(s^*)$ distribution computed from the time derivative of the concentration profile by the method of Stafford (see the Experimental Procedures). The concentration of tau is 7.5 ¿M, and the concentration of tubulin is 15 ¿M. This distribution was analyzed by DCDT+ software, with three Gaussian curves representing three sedimentation boundaries respectively in the plane line, dotted line, and dashed line. Open circles represent experimental values. The long dashed line represents the best fit curve. The inset shows the same analysis for tubulin alone (15 ¿M). (B) shows the percentage of three peaks area described above by DCDT+, with 6 S (b), 35 S (1) and 45 S (9) boundaries in the function of the tau/tubulin molar ratio for various concentration of tubulin: 15 ¿M (s); 10 ¿M (âââ), and 5 ¿M (- - -). The inset shows the variation of the apparent sedimentation coefficient in the function of the tau/tubulin ratio with tubulin 15 ¿M. This coefficient was obtained by analysis of the S^* distribution described above. Tau by itself does not contribute to the signal. Note that for 5 ¿M tubulin there is no 45 S boundary.

and remained constant from the tau/tubulin ratio of 0.5, which corresponds to one tau for two tubulin dimers. The most rapid sedimenting peak (45 S), which was absent for a tubulin concentration of 5 ¿M, appeared at a tau/tubulin ratio of 0.5 for a tubulin concentration of 10 ¿M (âââ) and at tau/tubulin ratio of 0.25 for a tubulin concentration of 15 ¿M (s). The formation of these different species is an equilibrium system, tubulin and tau concentration dependent.

To gain insight into the nature of the self-association process, we examined the samples by EM. They consisted of circular polymers that were mostly single wall rings with an average external diameter of about 45 ◐ 5 nm and an internal diameter of 30 ◐ 5 nm, corresponding to about 14

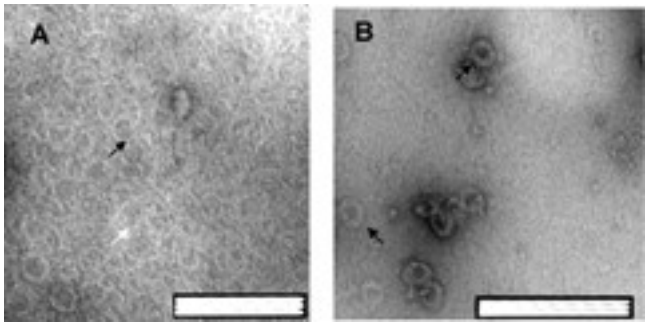

FIGURE 4: Electron micrographs of tau-induced tubulin oligomers at 20 °C. Ring structures at 20 °C for a tau/tubulin ratio of 1.2. In (A), the grid is covered with circular structures with single wall rings (white arrow) and possibly partial rings or spirals (black arrow), whereas in (B), thicker wall rings that might correspond to double rings are observed. The standard bar represents in both cases 200 nm.

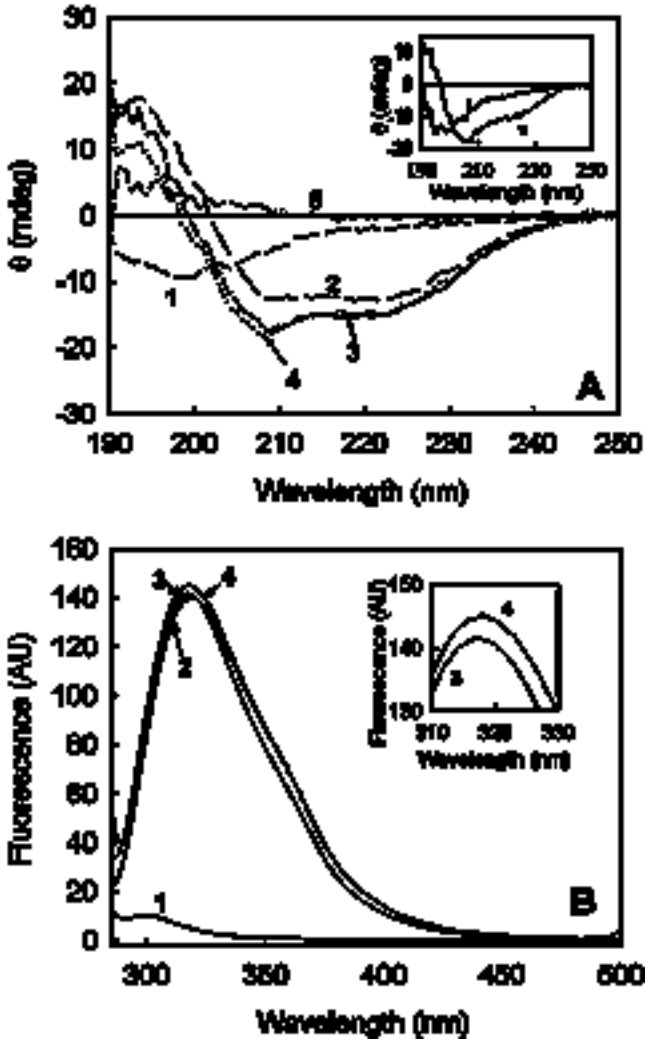

FIGURE 5: Spectrometric study of tau–tubulin interaction at 20 °C (A) Far-UV spectra of 10 μM tau (1), 10 μM tubulin (2), and 10 and 10 μM tau–tubulin mixture (3). (4) Linear combination of the separate spectra of tau and tubulin (4) 1 + 2). The difference between (3) and (4) is drawn in (5). Spectra were recorded in a 0.1 mm cuvette. The inset represents 2 μM tau spectra without TFE (1) or with 40% TFE (2). Spectra were recorded with a 1 mm cuvette with 2 μM tau. (B) Fluorescence spectra of 15 μM tau (1), 15 μM tubulin (2), and 15 and 15 μM tau–tubulin mixture (3). (4) Linear combination of the separate spectra of tau and tubulin (4) 1 + 2). The excitation wavelength is 275 nm. The inset represents an enlarged view of the peak area of (3) and (4). To clarify the inset, tubulin spectrum (2) was omitted.

tubulin dimer rings (Figure 4A). Nevertheless, the EM observation also revealed the presence of other circular polymers, such as thick wall rings and possibly spirals (Figure 4B), as well as partial rings. This structural heterogeneity could explain the spread profile of the peaks of the $g(s^*)$ distribution of the fast sedimenting species in the sedimentation velocity experiment (Figure 3A).

Because tau is unordered in solution, it has been frequently suggested that it might acquire some folding upon interaction with tubulin (*15*, *49*). Our results showed that tau interacted with tubulin and promoted tubulin oligomerization. To check for potential changes in the secondary structure accompanying these interactions, we performed CD measurements. Spectra obtained for tau without TFE (line 1 of the inset of Figure 5A) showed a minimum around 200 nm, which is characteristic of largely random-coil structures. In the presence of TFE, tau spectrum (line 2 of the inset of Figure 5A) presented a maximum at 190 nm and two minima at 208 and 222 nm, characteristic of R-helical structures. However, the tau interaction with tubulin did not change the spectra of the mixture substantially, arguing that the random-coil structure dominated in all cases. Indeed, the observed CD spectrum of a mixture of tau and tubulin (line 3 of Figure 5A) is almost superimposable on that obtained by a linear combination of the individual CD spectra of tau and tubulin in the same ratio (line 4 of Figure 5A). This indicates that there is no change in the overall helical-structure content of either tau or tubulin, resulting from the interaction. However, this does not rule out local changes at tau–tubulin or tubulin–tubulin binding interfaces.

Because tubulin and tau have aromatic residues, we also performed fluorescence experiments to further characterize their interaction. During complex formation, the fluorescence emission spectrum can shift in the wavelength of its maximum or in fluorescence intensity. These shifts can therefore be used to follow interactions. Figure 5B shows the uncorrected emission spectra of tau (line 1) and of tubulin (line 2). The fluorescence emission spectrum of a mixture of tau and tubulin (line 3) was shifted toward the lower wavelengths with a slight modification in its intensity as compared to the summed emission spectra of the two individual components (line 4 and inset of Figure 5B). This small change in fluorescence is compatible with a minor modification in the environment of tryptophan residues of tubulin. We conducted the same measurements with an excitation wavelength of 295 nm (data not shown). At this wavelength, the emission fluorescence signal was only due to tubulin, because tau has no tryptophan residues. Nevertheless, it did not improve the result significantly, nor did it permit any quantitative analysis of the interaction. Thus, at 20 °C, tau binds to tubulin with no apparent R-helical structure induction and induces tubulin assembly into rings.

Tau–Tubulin Interaction at 37 °C. Having shown that tau decreased the critical concentration in PEMGT buffer at 37 °C and that tau was able to induce the assembly of tubulin into rings at 20 °C in PGT buffer, we investigated tau–tubulin interactions at 37 °C in PGT buffer. PGT is a magnesium less buffer that normally supports neither tubulin association nor microtubule assembly in our range of tubulin

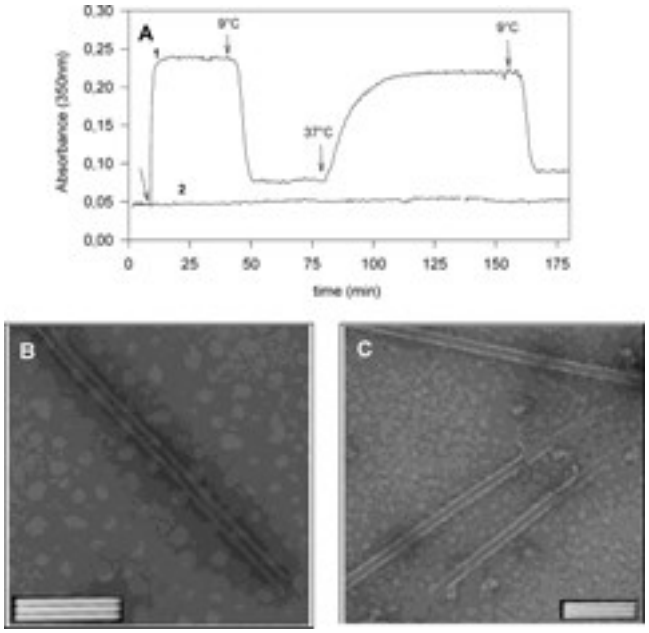

FIGURE 6: Tau−tubulin interaction at 37 °C. (A) Compared effect of tau and taxol on 6 ℓM tubulin in PGT buffer with 10^{-4} M GTP. Line 1 shows 2 cycles of assembly−disassembly upon addition of 5 ℓM tau (addition marked by the first arrow). Line 2 shows no assembly upon addition of equimolar taxol (addition marked by the first arrow). (B and C) Electron micrographs of tau-induced tubulin oligomers. (B) At 37 °C, we observe standard microtubules, whereas (C) at 25 °C, we see microtubules, which start to depolymerize, with protofilaments pealing outward at the microtubule ends. The bar represents 200 nm.

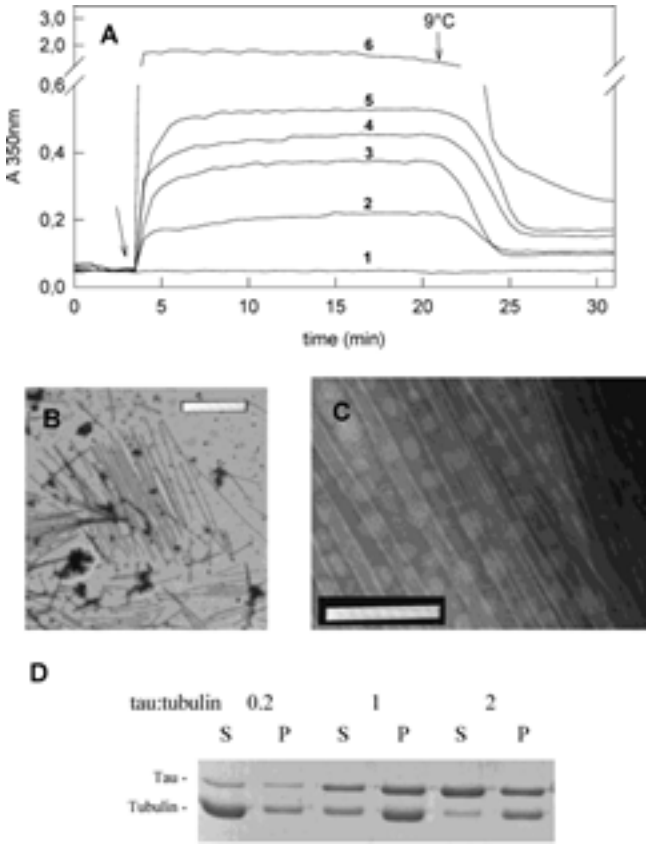

FIGURE 7: Tubulin assembly in the presence of tau in nonassembly conditions at 37 °C. (A) Effect of various concentrations of tau (1, 0 ℓM; 2, 3 ℓM; 3, 5 ℓM; 4, 7.5 ℓM; 5, 10 ℓM; and 6, 20 ℓM) on 10 ℓM tubulin in PGT buffer with 10^{-4} M GTP. Assembly was started by tau addition (first arrow), and disassembly was induced by switching the temperature to 9 °C. (B and C) Electron micrographs of tau-induced bundles at 37 °C, with the standard bar representing respectively 2 ℓm and 200 nm. (D) SDS−PAGE analysis of the interaction. Tubulin is constant (5 ℓM), and tau increased from 1 to 10 ℓM. Samples were centrifuged at 50 000 rpm (see the Experimental Procedures), and the supernatant (S) and pellet (P) were analyzed side by side to determine tau and tubulin concentrations in both fractions relative to itself. The upper band is tau, and the lower band is tubulin.

concentration (3−30 ℓM). However, at 37 °C, we observed an immediate increase in turbidity upon addition of tau, which implied the formation of polymers (line 1 of Figure 6A). Assembly was reversed by cooling the samples to 9 °C, which indicated the absence of irreversible aggregation. Disassembly was rapid and reached a new baseline within 5 min, slightly higher than the original baseline. From EM, we confirmed that these polymers observed at 37 °C were microtubules (Figure 6B). Upon cooling, the samples presented depolymerizing microtubules with ends pealing outward and even some rings (Figure 6C). At 9 °C, rings and a few residual cold-resistant microtubules were observed by EM, explaining the remaining turbidimetry. With 10^{-4} M GTP, tubulin was able to undergo several cycles of assembly−disassembly (two are shown in Figure 6A), whereas at 10^{-5} M GTP, only one cycle of assembly−disassembly was observed (data not shown). This indicated that GTP hydrolysis occurred during tau-induced microtubule formation and that tau was unable to induce microtubule formation from GDP−tubulin. Furthermore, to show the specificity of the tau effect in PGT buffer, we compared it to taxol in the same conditions. Line 2 of Figure 6A shows that equimolar taxol is not able to induce tubulin assembly in PGT buffer.

Titration of tubulin assembly by tau revealed interesting features. Upon increasing the concentration of tau to a 1:1 molar ratio, we observed a gradual increase of the turbidity plateau (Figure 7A). When tau concentration was greater than tubulin concentration, the turbidity signal increased dramatically to an absorbance greater that 2 (line 6 of Figure 7A). This drastic increase of turbidity correlated with the presence of bundles of microtubules as evidenced by EM (parts B and C of Figure 7). Turbidity is known to be a function of the total weight concentration of scattering particles only when the particles have small diameters compared to the wavelength of incident light (*50*, *51*). Bundles do not match these conditions, which explains the observed turbidimetric behavior of microtubules in these conditions.

To study the linkage of tau binding to tubulin isodesmic self-association, we thus used cosedimentation assays (see the Experimental Procedures) rather than turbidimetric measurements (Figure 7D). It enabled us to measure the concentration of microtubules and tau bound to microtubules in the pellet.

Analysis of Tau−Tubulin Interaction at 37 °C. We assumed in first approximation that tau concentration in the supernatant was equal to $[tau_{free}]$, tau concentration in the pellet, equal to $[tau_{bound}]$, and tubulin concentration in the supernatant, equal to $[tubulin_{free}]$, thus neglecting the quantity of potential small tau−tubulin complexes. This enabled us to quantitatively analyze tau binding. A number of theoretical studies have shown that in linked self-association systems, the shape of the ligand-binding isotherm depends on the

a longitudinal bridging of the tubulin dimers. Indeed, several studies have shown that tau would form oligomers or aggregates upon binding to microtubules, which is consistent with the hypothesis of an accumulation of tau on the microtubule surface (*61*, *62*).

It has been suggested that tau gets structured upon binding to its ligand. Kotani et al., by NMR (*49*), presented evidence of a disordered to ordered transition upon microtubule binding, suggesting also a particular involvement of tyrosines, which might be located in H12. We showed that unstructured tau was able to interact with CR(404−451), C*â*(394−445), or tubulin dimers, causing a slight shift in fluorescence intensity and wavelength, suggesting a small modification in the tryptophan environment. The specificity of the interaction of the C-terminal tubulin fragments was confirmed by the inhibition and disassembly of tau-induced microtubules. Maccioni et al. (*63*) described the interaction between tubulin CR(430−441) and C*â*(422−434) and two tau repeat domains R1 and R3, indicating that tubulin peptides induced structural changes in the tau R3 domain. Contrary to these results on small peptides, our CD analysis with entire tau and tubulin dimers has shown no significant folding upon binding as evidenced by CD of the tubulin−tau ring solutions (Figures 3 and 5). Moreover, our results are in agreement with another binding study performed on R3 and a different small *â* tubulin peptide (434−445), which revealed a lack of secondary structural modification upon interaction (*64*). We can thus conclude that recombinant tau does not need to gain a specific R-helical structure to bind to tubulin C-terminal. This is consistent with the very recent results of Santarella et al., who showed that tau retains most of its disordered structure when bound to tubulin−microtubules (*65*). Furthermore, we showed that the H11 and H12 belonging to CR and C*â*, which are suspected to bind specifically to tau, are sufficient for tau binding to the C-terminal peptides, and their helical folding does not seem necessary. This also could imply a role of the unstructured C-terminal tails in the binding via charge−charge interactions. Indeed, it has been shown previously that the C-terminal tails could also play a important role in MAP binding (*66*) and its regulation (*67*).

Finally, we showed that, contrary to taxol, tau is able to compensate for the absence of magnesium. A parallel can be drawn between tau and Mg^{2+}, which gives us new clues toward understanding the tau molecular mechanism of action. Magnesium is known to be an absolute requirement for tubulin assembly in vitro (*68*). It stabilizes both the R−*â* association in the tubulin heterodimer (*69*) and the *â*−R association between heterodimers (*70*). Tubulin dimer has several low-affinity and two high-affinity binding sites for Mg^{2+}. The first high-affinity magnesium ion is coordinated with the GTP bound to the N site of the R subunit at the R−R dimerization interface (*24*) and is necessary for the structural integrity of the tubulin dimer (*69*). The second one was proposed to be coordinated with the hydrolyzable GTP bound to the *â* subunit at the *â*−R-protofilament-forming interface in the E site. In our case, in PGT buffer, which did not contain any added Mg^{2+}, tau was able to induce tubulin self-association, whereas taxol, a well-known Mg^{2+}-dependent microtubule inducer (*71*), was unable to induce tubulin assembly. We thus measured the concentration of Mg^{2+} in our samples to evaluate the proportion of residual Mg^{2+} in tubulin. We detected 24 *í*M Mg^{2+} for 22 *í*M tubulin, i.e., roughly 1 Mg^{2+} per tubulin dimer, corresponding probably to the high-affinity Mg^{2+} of the N site. When this Mg^{2+}, necessary for the structure of tubulin dimer, was removed from the N site by the addition of 1 mM EDTA, the tau-induced tubulin self-association did not occur (data not shown). This indicates that tau does not substitute for the Mg^{2+} located in the N site. Instead, tau probably substitutes for either the Mg^{2+} of the E site or a low-affinity binding site. In conclusion, tau substitutes for magnesium and, by means of a completely different mechanism consisting of binding to the C-terminal domains of tubulin monomers, stabilizes the longitudinal protofilament-forming interactions among tubulin molecules. This induces tubulin self-association into rings at 20 °C or microtubules at 37 °C.

This tau−tubulin interaction study was conducted in minimal conditions as a model system that does not take into consideration the numerous post-translational modifications that tau may undergo in the cell, such as phosphorylation. Nevertheless, it was the prerequisite step to understand the molecular basis of the tau-stabilizing effect on microtubule cytoskeleton. Now, we will be able to study the effect of post-translational tau modifications or mutations and the effect of molecular crowding on this system.

ACKNOWLEDGMENT

We are very grateful to Dr. M. Goedert (MRC, Cambridge, U.K.) for htau40 plasmid, M. LÂpez (Santiago, Chile) for peptide purification, and P. Lopez Navajas and Dr. G. Rivas (CIB, Madrid, Spain) for the divalent cation measurements, as well as Pr. J. M. Verdier (EPHE, Montpellier, France) and Svetlana Gorokhova (Rockefeller University, New York) for helpful discussion.

REFERENCES

1. Cleveland, D. W., Hwo, S. Y., and Kirschner, M. W. (1977) Purification of tau, a microtubule-associated protein that induces assembly of microtubules from purified tubulin, *J. Mol. Biol. 116*, 207−225.
2. Trojanowski, J. Q., and Lee, V. M. (2002) The role of tau in Alzheimer's disease, *Med. Clin. North Am. 86* (3), 615−627.
3. Buee, L., Bussiere, T., Buee-Scherrer, V., Delacourte, A., and Hof, P. R. (2000) Tau protein isoforms, phosphorylation, and role in neurodegenerative disorders, *Brain Res. Rev. 33* (1), 95−130.
4. Mandelkow, E. M., Stamer, K., Vogel, R., Thies, E., and Mandelkow, E. (2003) Clogging of axons by tau, inhibition of axonal traffic, and starvation of synapses, *Neurobiol. Aging 24* (8), 1079−1085.
5. Panda D, Samuel J. C., Massie M., Feinstein S. C., and Wilson L. (2003) Differential regulation of microtubule dynamics by three- and four-repeat tau: Implications for the onset of neurodegenerative disease, *Proc. Natl. Acad. Sci. U.S.A. 100* (16), 9548−9553.
6. Lee, G., Cowan, N., and Kirschner, M. (1988) The primary structure and heterogeneity of tau protein from mouse brain, *Science 239* (4837), 285−288.
7. Goode, B. L., and Feinstein, S. C. (1994) Identification of a novel microtubule binding and assembly domain in the developmentally regulated inter-repeat region of tau, *J. Cell Biol. 124* (5), 769−782.
8. Gustke, N., Trinczek, B., Biernat, J., Mandelkow, E. M., and Mandelkow, E. (1994) Domains of tau protein and interactions with microtubules, *Biochemistry 33* (32), 9511−9522.
9. Goode, B. L., Denis, P. E., Panda, D., Radeke, M. J., Miller, H. P., Wilson, L., and Feinstein, S. C. (1997) Functional interactions between the proline-rich and repeat regions of tau enhance microtubule binding and assembly *Mol. Biol. Cell 8*(2), 353−365.

10. Littauer, U. Z., Giveon, D., Thierauf, M., Ginzburg, I., and Ponstingl, H. (1986) Common and distinct tubulin binding sites for microtubule-associated proteins *Proc. Natl. Acad. Sci. U.S.A. 83*(19), 7162−7166.
11. Serrano, L., Montejo de Garcini, E., Hernandez, M. A., and Avila, J. (1985) Localization of the tubulin binding site for tau protein *Eur. J. Biochem. 153*(3), 595−600.
12. Marya, P. K., Syed, Z., Fraylich, P. E., and Eagles, P. A. (1994) Kinesin and tau bind to distinct sites on microtubules *J. Cell Sci. 107* (Pt 1), 339−344.
13. Maccioni, R. B., Rivas, C. I., and Vera, J. C. (1988) Differential interaction of synthetic peptides from the carboxyl-terminal regulatory domain of tubulin with microtubule-associated proteins *EMBO J. 7*(7), 1957−1963.
14. Chau, M. F., Radeke, M. J., De Ines, C., Barasoain, I., Kohlstaedt, L. A., and Feinstein, S. C. (1998) The microtubule-associated protein tau cross-links to two distinct sites on each alpha and beta tubulin monomer via separate domains *Biochemistry 37*(51), 17692−17703.
15. Al-Bassam, J., Ozer, R. S., Safer, D., Halpain, S., and Milligan, R. A. (2002) MAP2 and tau bind longitudinally along the outer ridges of microtubule protofilaments *J. Cell Biol. 157*(7), 1187−1196.
16. Kar, S., Fan, J., Smith, M. J., Goedert, M., and Amos, L. A. (2003) Repeat motifs of tau bind to the insides of microtubules in the absence of taxol *EMBO J. 22*(1), 70−7.
17. Devred, F., Douillard, S., Briand, C., and Peyrot, V. (2002) First tau repeat domain binding to growing and taxol-stabilized microtubules, and serine 262 residue phosphorylation *FEBS Lett. 523* (1−3), 247−251.
18. Butner, K. A., and Kirschner, M. W. (1991) Tau protein binds to microtubules through a flexible array of distributed weak sites *J. Cell Biol. 115*(3), 717−730.
19. Novella, I. S., Andreu, J. M., and Andreu, D. (1992) Chemically synthesized 182−235 segment of tau protein and analogue peptides are efficient in vitro microtubule assembly inducers of low apparent sequence specificity *FEBS Lett. 311*(3), 235−40.
20. Ichihara, K., Kitazawa, H., Iguchi, Y., Hotani, H., and Itoh, T. J. (2001) Visualization of the stop of microtubule depolymerization that occurs at the high-density region of microtubule-associated protein 2 (MAP2) *J. Mol. Biol. 312*(1), 107−118.
21. Ennulat, D. J., Liem, R. K., Hashim, G. A., and Shelanski, M. L. (1989) Two separate 18-amino acid domains of tau promote the polymerization of tubulin *J. Biol. Chem. 264*(10), 5327−30.
22. Aizawa, H., Kawasaki, H., Murofushi, H., Kotani, S., Suzuki, K., and Sakai, H. (1989) A common amino acid sequence in 190-kDa microtubule-associated protein and tau for the promotion of microtubule assembly *J. Biol. Chem. 264*(10), 5885−90.
23. Jimenez, M. A., Evangelio, J. A., Aranda, C., Lopez-Brauet, A., Andreu, D., Rico, M., Lagos, R., Andreu, J. M., and Monasterio, O. (1999) Helicity of alpha(404−451) and beta(394−445) tubulin C-terminal recombinant peptides *Protein Sci. 8*(4), 788−799.
24. Lowe, J., Li, H., Downing, K. H., and Nogales, E. (2001) Refined structure of alpha beta-tubulin at 3.5 A resolution *J. Mol. Biol. 313*(5), 1045−1057.
25. Weisenberg, R. C., Borisy, G. G., and Taylor, E. W. (1968) The colchicine-binding protein of mammalian brain and its relation to microtubules *Biochemistry 7*, 4466−4479.
26. Andreu, J. M., Gorbunoff, M. J., Lee, J. C., and Timasheff, S. N. (1984) Interaction of tubulin with bifunctional colchicine analogues: an equilibrium study *Biochemistry 23*, 1742−1752.
27. Deleage, G., Blanchet, C., and Geourjon, C. (1997) Protein structure prediction. Implications for the biologist *Biochimie 79*(11), 681−686.
28. Barbier, P., Gregoire, C., Devred, F., Sarrazin, M., and Peyrot,V. (2001) In vitro effect of cryptophycin 52 on microtubule assembly and tubulin: molecular modeling of the mechanism of action of a new antimitotic drug *Biochemistry 40*(45), 13510−13519.
29. Minton, A. P. (1994) *Modern Ultracentrifugation* (Schuster, T. M., and Laue, T. M. Eds.) pp 81−93, Birkhauser, Boston.
30. Johnson, M. L., Correia, J. J., Yphantis, D. A., and Halvorson, H. R. (1981) Analysis of data from the analytical ultracentrifuge by nonlinear least-squares techniques *Biophys. J. 36*, 575−588.
31. Laue, T. M., Shah, B. D., Ridgeway, T. M., and Pelletier, S. L. (1992) Computer-aided interpretation of analytical sedimentation data for proteins in *Analytical Ultracentrifugation in Biochemistry and Polymer Sciences* (Harding, S. E., Rowe, A. J. & Horton, J. C., eds), pp 90−125. Royal Society of Chemistry, Cambridge, UK.
32. Schuck, P., and Rossmanith, P. (2000) Determination of the sedimentation coefficient distribution by least-squares boundary modeling *Biopolymers 54*, 328−341.
33. Bloomfield, V., Van Holde, K. E., and Dalton, W. O. (1967) Frictional coefficients of multisubunit structures. II. Application to proteins and viruses *Biopolymers. 5*(2), 149−159.
34. Stafford, W. F., III (1992) in Modern Applications of Analytical Ultracentrifugation in *Analytical Ultracentrifugation in Biochemistry and Polymer Science* (Harding, S. E., Rowe, A. J. & Horton, J. C., eds), pp359−393, The royal Society of Chemistry, Cambridge, UK.
35. Philo, J. S. (2000) A method for directly fitting the time derivative of sedimentation velocity data and an alternative algorithm for calculating sedimentation coefficient distribution functions *Anal. Biochem. 279*(2), 151−163.
36. Diaz, J. F, Menendez, M., Andreu, J. M. (1993) Thermodynamics of ligand-induced assembly of tubulin. *Biochemistry. 32*(38), 10067−77.
37. Buey, R. M., Diaz, J. F., Andreu, J. M., O'Brate A., Giannakakou P., Nicolaou, K. C., Sasmal, P. K., Ritzen, A., Namoto, K. (2004) Interaction of Epothilone Analogues with the Paclitaxel Binding Site: Relationship between Binding Affinity, Microtubule Stabilization, and Cytotoxicity *Chemistry & Biology 11*, 225−236.
38. Martin, M. T., and Shapiro, R. (1988) Atomic absorption spectrometry of magnesium *Methods Enzymol. 158*, 365−70.
39. Rivas, G., Lopez, A., Mingorance, J., Ferrandez, M. J., Zorrilla, S., Minton, A. P., Vicente, M., and Andreu, J. M. (2000) Magnesium-induced linear self-association of the FtsZ bacterial cell division protein monomer. The primary steps for FtsZ assembly *J. Biol. Chem. 275*(16), 11740−9.
40. Barbier, P., Peyrot, V., Leynadier, D., and Andreu, J. M. (1998) The active GTP- and ground GDP-liganded states of tubulin are distinguished by the binding of chiral isomers of ethyl 5-amino-2-methyl-1,2-dihydro-3-phenylpyrido[3,4-b] pyrazin-7-yl carbam-ate *Biochemistry 37*, 758−768.
41. Ruben, G. C., Ciardelli, T. L., Grundke-Iqbal, I., and Iqbal, K. (1997) Alzheimer disease hyperphosphorylated tau aggregates hydrophobically *Synapse 27*, 208−229.
42. Wille, H., Drewes, G., Biernat, J., Mandelkow, E. M., and Mandelkow, E. (1992) Alzheimer-like paired helical filaments and antiparallel dimers formed from microtubule-associated protein tau in vitro *J. Cell Biol. 118*(3), 573−584.
43. Weingarten, M. D., Lockwood, A. H., Hwo, S. Y., and Kirschner, M. W. (1975) A protein factor essential for microtubule assembly *Proc. Natl. Acad. Sci. U.S.A. 72*, 1858−1862.
44. Schweers, O., Schönbrunn-Hanebeck, E., Marx, A., and Mandelkow, E. (1994) Structural studies of tau protein and Alzheimer paired helical filaments show no evidence for beta-structure *J. Biol. Chem. 269*, 24290−24297.
45. Syme, C. D., Blanch, E. W., Holt, C., Jakes, R., Goedert, M., Hecht, L., and Barron, L. D. (2002) A Raman optical activity study of rheomorphism in caseins, synucleins and tau. New insight into the structure and behavior of natively unfolded proteins *Eur. J. Biochem. 269*, 148−156.
46. Le Maire, M., Rivas, E., and Moller, J. V. (1980) Use of gel chromatography for determination of size and molecular weight of proteins: further caution *Anal. Biochem. 106*, 12−21.
47. Tanford, C., Kawahara. K., Lapanje, S., Hooker, T. M., Jr., Zarlengo, M. H., Salahuddin, A., Aune, K. C., and Takagi, T. (1967) Proteins as random coils. 3. Optical rotatory dispersion in 6 M guanidine hydrochloride *J Am Chem Soc. 89*(19), 5023−9.
48. Lee, J. C., Rajendran, S. (1994) Studies of macromolecular interaction by sedimentation velocity in *Modern Analytical Ultracentrifugation* (Schuster, T. M., and Laue, T. M., eds), pp. 138−155, Birkhauser, Boston.
49. Kotani, S., Kawai, G., Yokoyama, S., and Murofushi, H. (1990) Interaction mechanism between microtubule-associated proteins and microtubules. A proton nuclear magnetic resonance analysis on the binding of synthetic peptide to tubulin *Biochemistry 29*(43), 10049−10054.
50. Berne, B. J. (1974) Interpretation of the light scattering from long rods *J. Mol. Biol. 89*(4), 755−758.
51. Gaskin, F. (1982) Techniques for the study of microtubule assembly in vitro *Methods Enzymol. 85* Pt B: 433−9.
52. Scatchard, G. (1949) The attractions of proteins for small molecules and ions *Ann. N.Y. Acad. Sci. 51*, 660−72.
53. Na, G. C., and Timasheff, S. N. (1985) Measurement and analysis of ligand-binding isotherms linked to protein self-associations *Methods Enzymol. 117*, 496−519.

54. Oosawa, F., and Asakura, S. (1975) Thermodynamics of the Polymerization of Protein, Academic Press, London, New York.
55. Na, G. C., and Timasheff, S.N. (1985) Velocity sedimentation study of ligand-induced protein self-association *Methods Enzymol. 117*, 459–95.
56. Scheele, R. B., and Borisy, G. G. (1979) In vitro assembly of microtubules in *Microtubules* (Roberts, K., and Hyams, J. S., Eds) pp 175–253, Academic Press, London.
57. Kirschner, M. W., Williams, R. C., Weingarten, M., Gerhart, J. C. (1974) Microtubules from mammalian brain: some properties of their depolymerization products and a proposed mechanism of assembly and disassembly *Proc. Natl. Acad. Sci. U.S.A. 71*(4), 1159–63.
58. Nogales, E., Wang, H. W., and Niederstrasser, H. (2003) Tubulin rings: which way do they curve? *Curr. Opin. Struct. Biol. 13*(2), 256–61.
59. Diaz, J. F., Pantos, E., Bordas, J., and Andreu, J. M. (1994) Solution structure of GDP-tubulin double rings to 3 nm resolution and comparison with microtubules *J. Mol. Biol. 238*(2), 214–25.
60. Doenges, K. H., Biedert, S., and Paweletz, N. (1976) Characterization of 20S component in tubulin from mammalian brain. *Biochemistry 15*(14), 2995–9.
61. Ackmann, M., Wiech, H., and Mandelkow, E. (2000) Nonsaturable binding indicates clustering of tau on the microtubule surface in a paired helical filament-like conformation *J Biol Chem. 275*(39), 30335–43.
62. Makrides, V., Shen, T. E., Bhatia, R., Smith, B. L., Thimm, J., Lal, R., and Feinstein, S. C. (2003) Microtubule-dependent oligomerization of tau. Implications for physiological tau function and tauopathies *J. Biol. Chem. 278*(35), 33298–304.
63. Maccioni, R. B., Vera, J. C., Dominguez, J., and Avila, J. (1989) A discrete repeated sequence defines a tubulin binding domain on microtubule-associated protein tau *Arch. Biochem. Biophys. 275*(2), 568–579.
64. Hoffmann, R., Dawson, N. F., Wade, J. D., and Otvos, L., Jr. (1997) Oxidized and phosphorylated synthetic peptides corresponding to the second and third tubulin-binding repeats of the tau protein reveal structural features of paired helical filament assembly, *J. Pept. Res. 50* (2), 132–142.
65. Santarella, R. A., Skiniotis, G., Goldie, K. N., Tittmann, P., Gross, H., Mandelkow, E. M., Mandelkow, E., and Hoenger, A. (2004) Surface-decoration of microtubules by human tau, *J. Mol. Biol. 339* (3), 539–553.
66. Mejillano, M. R., and Himes, R. H. (1991) Assembly properties of tubulin after carboxyl group modification, *J. Biol. Chem. 266* (1), 657–664.
67. Boucher, D., Larcher, J. C., Gros, F., and Denoulet, P. (1994) Polyglutamylation of tubulin as a progressive regulator of in vitro interactions between the microtubule-associated protein tau and tubulin, *Biochemistry 33* (41), 12471–12477.
68. Lee, J. C., and Timasheff, S. N. (1977) In vitro reconstitution of calf brain microtubules: Effects of solution variables, *Biochemistry 16* (8), 1754–1764.
69. Menendez, M., Rivas, G., Diaz, J. F., and Andreu, J. M. (1998) Control of the structural stability of the tubulin dimer by one high affinity bound magnesium ion at nucleotide N-site, *J. Biol. Chem. 273* (1), 167–176.
70. Vulevic, B., and Correia, J. J. (1997) Thermodynamic and structural analysis of microtubule assembly: The role of GTP hydrolysis, *Biophys. J. 72* (3), 1357–1375.
71. Howard, W. D., and Timasheff, S. N. (1988) Linkages between the effects of taxol, colchicine, and GTP on tubulin polymerization, *J. Biol. Chem. 263* (3), 1342–1346.